This is a repository copy of *Investigation of a steel connection to accommodate ductility demand of beams in fire*.

White Rose Research Online URL for this paper:
http://eprints.whiterose.ac.uk/142918/

Version: Accepted Version

Article:
Liu, Y., Huang, S. orcid.org/0000-0003-2816-7104 and Burgess, I. orcid.org/0000-0001-9348-2915 (2019) Investigation of a steel connection to accommodate ductility demand of beams in fire. Journal of Constructional Steel Research, 157. pp. 182-197. ISSN 0143-974X

https://doi.org/10.1016/j.jcsr.2019.02.029

Article available under the terms of the CC-BY-NC-ND licence (https://creativecommons.org/licenses/by-nc-nd/4.0/).

Reuse
This article is distributed under the terms of the Creative Commons Attribution-NonCommercial-NoDerivs (CC BY-NC-ND) licence. This licence only allows you to download this work and share it with others as long as you credit the authors, but you can't change the article in any way or use it commercially. More information and the full terms of the licence here: https://creativecommons.org/licenses/

Takedown
If you consider content in White Rose Research Online to be in breach of UK law, please notify us by emailing eprints@whiterose.ac.uk including the URL of the record and the reason for the withdrawal request.

eprints@whiterose.ac.uk
https://eprints.whiterose.ac.uk/

INVESTIGATION OF A STEEL-CONNECTION TO ACCOMMODATE DUCTILITY DEMAND OF BEAMS IN FIRE

Yu Liu[1*], Shan-Shan Huang[1] and Ian Burgess[1]

[1]*Department of Civil and Structural Engineering, University of Sheffield, Mappin Street, Sheffield S1 3JD, United Kingdom.*

*Corresponding Author: E-mail address: yliu230@sheffield.ac.uk (Yu Liu)

ABSTRACT

In fire conditions the provision of connection ductility is key to the prevention of brittle failure and progressive collapse of steel and steel-concrete composite framed structures. This paper describes the development and testing of a novel connection concept intended to provide appropriate ductility enhancement compared to that of conventional connection types. The connection consists of two connection pieces, each of which takes the form of a web cleat which includes a semi-cylindrical section. This section allows the beam-end to move towards or away from the column-face by deforming plastically. A simplified analytical model has been developed to simulate the mechanical behaviour of the proposed connection, and this model will eventually enable the incorporation of this new connection type into global frame analysis to be used in performance-based structural fire engineering design. The model has been tested against FEA simulations and against model-scale experiment results, indicating that it can predict the behaviour of the connection with satisfactory accuracy. Preliminary sub-frame analysis results indicate that the proposed connection behaves similarly to an idealized pinned connection under ambient-temperature conditions, but provide significantly larger ductility, and resistance to disproportionate collapse, compared to conventional connection types.

Key words: Connections; fire; robustness; ductility demand

1. INTRODUCTION

Fire accidents occur frequently around the world and cause both human casualties and substantial losses. Elevated temperatures usually cause degradation of the structural properties of commonly-used construction materials, especially those of steel. Therefore, the resistance of structures to disproportionate collapse in fire needs to be given sufficient attention during their design stage. It is traditionally assumed that connections have sufficient fire resistance, on the basis that they tend to experience lower temperatures than the members which they connect. However, connection failures which occurred in the collapse of the World Trade Centre buildings in New York [1] and in the Cardington full-scale fire tests [2] showed that connections are actually the most vulnerable structural elements, and that their fractures may trigger the collapse of floors and the buckling of columns; this has the capacity to cause the disproportionate collapse of an entire building [3]. In maintaining structural integrity and preventing progressive collapse, connections play a very important role by acting as the critical components tying all other structural members together. The behaviour of connections at elevated temperatures differs from that at ambient temperature. The internal forces experienced by connections in fire can broadly be classified into four stages. In the initial stage, at ambient temperature, the major force carried is vertical shear accompanied by some bending moment depending on the details of the connection, due to the design loading carried by the beams. After heating starts, a connection begins to experience additional compression normal to the column face due to the restrained thermal expansion of the connected beam at a stage when weakening of the beam's material is not very

significant. Eventually, at very high temperature, when material weakening becomes more important than thermal expansion, the connected beam carries its load mainly by catenary action, and the connections become subject to tension. In cooling, from either of the two previous stages, the thermal contraction of the beam as it regains stiffness superposes tensile force on the connection. However, the first generation of fire tests on connections concentrated on their rotational characteristics at high temperatures. The first experimental fire tests, on six different types of connection, were conducted by Kruppa [4]. These tests aimed mainly to establish the performance of high-strength bolts, and the behaviour of the joints themselves was not presented. The global rotational behaviour of a limited number of joints exposed to the ISO834 Standard Fire was first studied by Lawson [5, 6]. Experiments done by Leston-Jones [7] on the full moment-rotation-temperature behaviour of flush endplate steel beam-to-column connections confirmed that their stiffness and strength decreased with the increase of temperature. In a following project Al-Jabri [8] continued this work for full-scale steel and composite connections derived from the Cardington building fire tests, and conducted studies of the effect of parameters including member size, connection type and failure mechanism. Ai-Jabri established that such experiments on isolated joints could not realistically represent the behaviour of joints within a structural frame, due to the lack of simultaneous axial force. Furthermore, experimental investigations, especially at elevated temperatures, are very expensive. Given the large variety of connections and the possible combinations of moment, rotation, axial force and axial displacement at any temperature, the total number of tests required to populate a meaningful database would

have been excessive. It became apparent that numerical simulation would be necessary to extend both the breadth and depth of the experimental studies. Liu [9] developed a three-dimensional numerical model including deterioration of material properties with temperature, non-uniform thermal expansion and large deformations, to simulate the response of steel connections in fire. Elsawaf [10] used the general-purpose Abaqus software to simulate the behaviour of steel beam-to-CFT columns connected by reverse-channel connections in fire. These approaches can produce accurate representations of the behaviour of connections but are computationally extremely burdensome; using this approach in the context of full-structure or structural subframe modelling is extremely time-consuming, both in model creation and in runtime. A component-based approach is more practical, although less accurate. This approach divides a connection into components which represent the actions of distinct structural zones; each component is idealized as a nonlinear "spring" of known characteristics. The component-based method provides a computationally cost-efficient alternative to detailed FE modelling. Da Silva [11] proposed an analytical procedure to predict the moment–rotation response of connections in fire which incorporates the variation of material properties of different components with the increase of temperatures. At the University of Sheffield, a systematic process to develop a high-temperature nonlinear component-based modelling approach has been conducted through a series of research projects[12-26], both experimental and theoretical. These have characterised the components of some current connections and have validated component-based models of these at elevated temperatures. Among these Yu [19] proposed and validated a yield-line-

based model for end-plate connections, and Dong [25] developed a model for reverse-channel connections following a similar approach. Dong [26] also developed a general-purpose component-based connection element for structural fire analysis and implemented this in the software Vulcan. This general-purpose element can combine temperature-dependent component characterizations, both in series (within individual bolt rows) and in parallel (as a collection of bolt rows and other significant locations) to create a two-noded element which is located between beam-end and a column node. The effect of cooling on component characterisations [16] is also included within this element.

However, conventional connection types lack the axial ductility to accommodate either the compressive or tensile axial forces mentioned above, and this could allow connection fractures to take place. Once fracturing of key components within a connection occurs, the connected beam can be detached from the supporting column, leading to an increase in the column's slenderness and thus to potential column buckling. This can lead to a sequence of failures which result in collapse of the whole structure. Connection failures could also trigger the collapse of slabs and the spread of fire into adjacent compartments. This research aims to develop a novel ductile connection which allows the large tensile and compressive deformations imposed by the connected beam at elevated temperatures, so as to reduce the connection forces generated and prevent connection fracture in fire. This paper illustrates the development of this new ductile connection. The analytical tensile and compressive model of the connection components has been developed on the basis of simple plastic theory, and the rotational model is achieved using an array of these components. The analytical model is

compared against Abaqus finite element simulations at both ambient and elevated temperatures and against experiments at ambient temperature. A simple case study tests the performance of the connection in a structural subframe.

2. DUCTILITY DEMAND AND DESIGN OF NOVEL DUCTILE CONNECTION

Connections are restrained by adjacent structural members. As described previously, during the initial stage of a fire accident a beam will apply axial compressive force to its connections due to restraint to its free thermal expansion. When the temperature increases further, and the beam has lost most of its bending resistance, tensile force will be applied to the connection due to the catenary action of the beam. The examples presented in Figure 1 illustrate this change in axial internal force acting on the connection. The difference between Figure 1(a) and 1(b) is that the free thermal expansion of the beam in Figure 1(b) is accommodated by ductile boundary conditions, so that both the compression and tension forces generated in (b) are much smaller than those in (a).

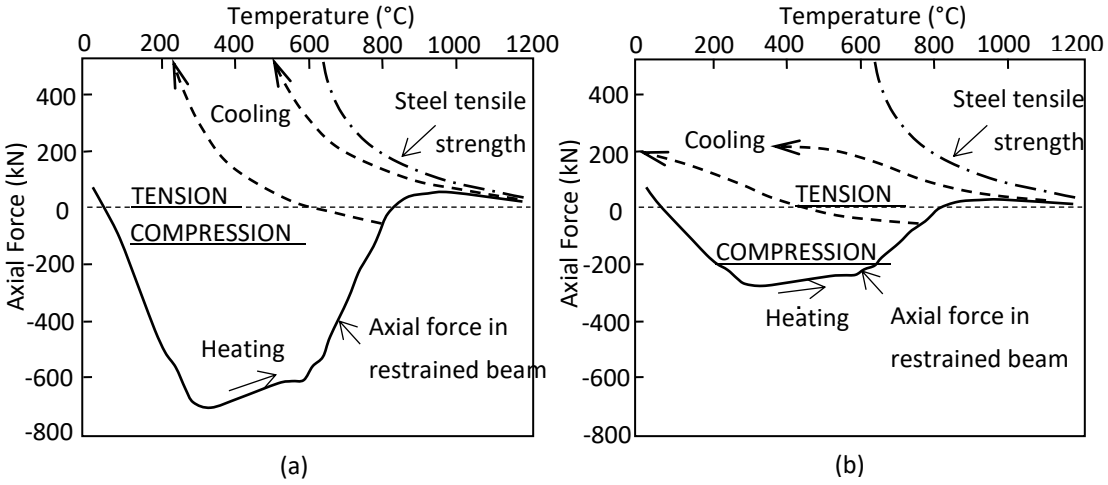

Figure 1. The change of axial internal forces of a connection in fire conditions [27]; (a) with strong axial restraint, (b) with axially ductile connections.

It is clear that a structure requires connections with high ductility in order to retain its integrity and stability under exposure to fire. The design of a proposal for an appropriate ductile connection is therefore governed firstly by the degree of ductility required. In the early stage of a fire, usually while the beam temperature is below about 600°C, the connection should be able to accommodate the thermal expansion of the connected beam, together with the effects of beam-end rotation and effective shortening due to beam deflection. This reduces the force transmitted to the adjacent structure and prevents connection fracture in compression. As shown in Figure 2(a), the bottom end of the connection should be able to withstand the horizontal movement:

$$\Delta_{\text{low-temp}} = \frac{1}{2}(\alpha \mathrm{l} \mathrm{T} + \mathrm{h}\theta) - \frac{4}{3}\delta^2 / \mathrm{l} \qquad (1)$$

Where α is the thermal expansion coefficient of steel, T is the beam temperature, l is the length of the beam, h is the height of the beam section and δ is the mid-span deflection of the beam.

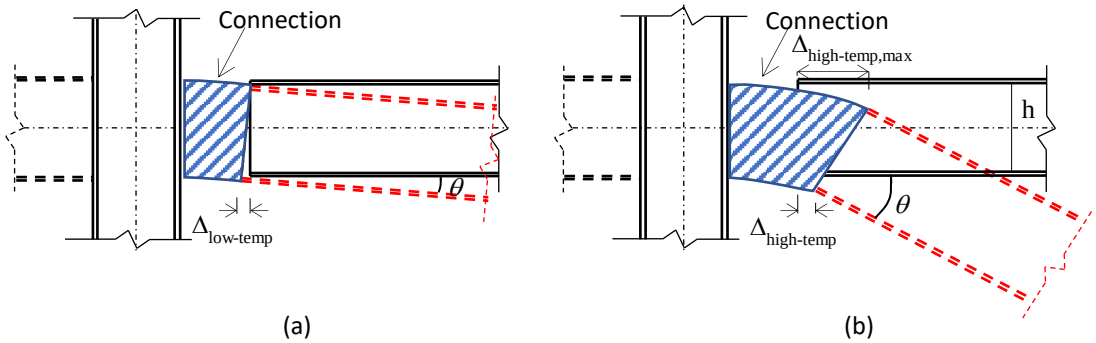

(a) (b)

Figure 2. Beam-end movements in different temperature phases; (a) Low-temperature movement, (b) High-temperature movement.

In the high temperature range, when the beam acts essentially in catenary action, the top edge of the connection should be able to accommodate a movement $\Delta_{\text{high-temp,max}}$ to prevent

fracture at the top of the connection and to avoid hard contact between the beam bottom flange and column face, as shown in Figure 2(b). Deformation $\Delta_{\text{high-temp,max}}$ and $\Delta_{\text{high-temp}}$ can be calculated using Equations (2) and (3). Furthermore, the connection should be able to withstand the tensile force generated by the catenary action of the beam, which can be calculated according to Equation (4), in which w_f is the uniformly distributed line load intensity. The deformability provided in tension effectively reduces the tensile force in the connection, especially when the beam is subject to large deflection, and this in turn helps to prevent connection fracture.

$$\Delta_{\text{high-temp}} = \frac{4}{3}\delta_{\max}{}^2 / l - \frac{1}{2}(\alpha l T + h\theta) \tag{2}$$

$$\Delta_{\text{high-temp,max}} = \frac{4}{3}\delta_{\max}{}^2 / l - \frac{1}{2}(\alpha l T - h\theta) \tag{3}$$

$$F = w_f l^2 / 8\delta_{\max} \tag{4}$$

To meet this prescribed ductility demand presented by the beam behaviour, taking into account ease of construction, the connection shown in Figure 3 is proposed. Advantages such as low cost and ease of installation currently make fin-plate and end-plate connections popular within the construction industry. The new connection consists of two identical parts, which can be considered as shaped web cleats. Each cleat includes; a fin-plate, bolted to the beam web; an end-plate, bolted to either the column web or flange, and; a semi-cylindrical section (which is either circular or elliptical in shape) between the fin-plate and end-plate. These deformed cleats can be fabricated by bending a steel plate. An alternative fabrication method might be to weld two plates to a semi-tubular section, which is a costlier and more labour intensive, and therefore not preferred. The semi-cylindrical section is the key to

providing the required push-pull ductility, allowing the fin-plate to move towards and away from the end-plate in order to accommodate the thermal expansion and catenary action of the connected beam, in surviving the different force conditions as the beam temperature rises. This is intended to enable the connection to resist large tensile and compressive deformations and to minimise the probability of brittle failure modes that may initiate progressive collapse.

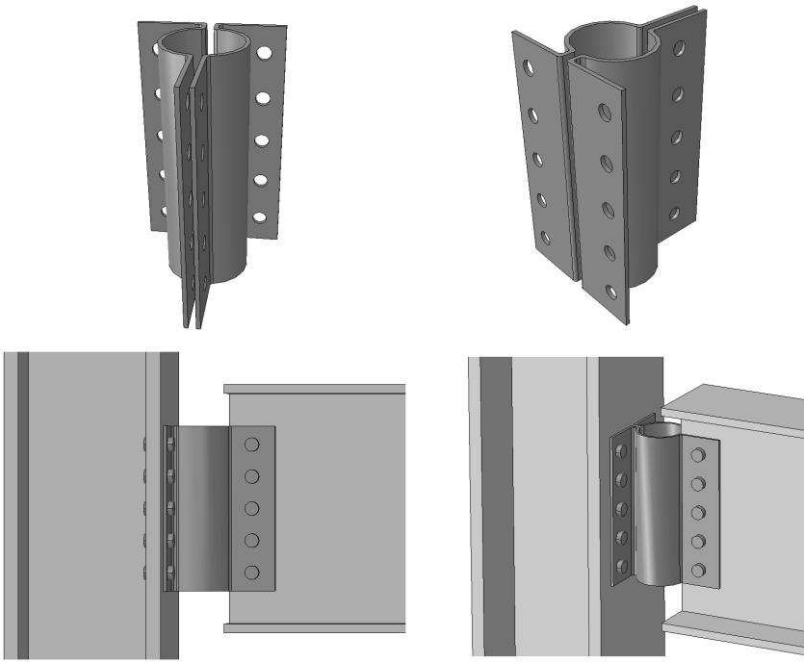

Figure 3. The proposed detail of the novel ductile connection.

As mentioned above, the cylindrical section should be able to accommodate the deformation of the connected beam during fire within both the low-temperature and high-temperature ranges. The diameter of the cylindrical section is a critical design parameter, which has the greatest impact on the ductility of the whole connection, and should be selected according to the values of $\Delta_{\text{low-temp}}$, $\Delta_{\text{high-temp,max}}$ and $\Delta_{\text{high-temp}}$. The example design demonstrated here is for a beam of length 7.5m, subject to a uniform line load at the Fire Limit State of 32.6 kN/m. The beam is designed to be UKB 533*210*109. The fin-plate and end-plate of the ductile

connection have been designed to the Eurocode. The dimensions of the connection are shown in Figure 4, and M20 Grade 8.8 bolts in 22mm diameter bolt holes are adopted. The ductile cylindrical section of the novel connection type will accommodate the large deflection of the connected beam at high temperature, which in turn significantly reduces the axial force in the connection. Therefore, the tensile forces in the welds and bolts will be modest. They will mainly take shear, which they are designed to Eurocode to take, and so they are not expected to be critical in this case. It is sized to satisfy Equations (1)-(3). When the temperature of the beam is 600°C $\Delta_{\text{low-temp}}$ of the beam is 29 mm. When its temperature reaches 800°C the catenary force is governed by the reduced tensile strength of the beam. Therefore, the maximum beam deflection $\delta_{\max}$, which is 548 mm, can be calculated according to Equation (4), and is then substituted into Equations (2) and (3) to calculate the axial deformation of the beam. The movements $\Delta_{\text{high-temp,max}}$ and $\Delta_{\text{high-temp}}$ of the beam at 800°C are 57mm and 22mm, respectively. Therefore, if the beam is designed to resist a temperature of 800°C, the connection should be able to accommodate at least 50 mm axial deformation. If the inner radius of the cylindrical section is designed to be 50mm, this enables the cylindrical section to have enough deformability to accommodate the axial deformations of the beam in both directions. The connection must, of course, be adequate for ambient-temperature Ultimate Limit State conditions. This involves checking shear capacity of the cylindrical section using Equation (5), and verifying the resistance of the connection according to BS EN1993-1-8 [28] at ambient temperature, under:

- bolt shear,

- bolt bearing,
- shear and bearing of the fin-plate,
- shear and bearing of the bolt group,
- shear of the end-plate.

$$V_{Rd} = A_v \frac{f_y}{\sqrt{3}\gamma_{M0}} \quad (5)$$

Where V_{Rd} and A_v are respectively the shear capacity and cross-sectional area of the cylindrical section.

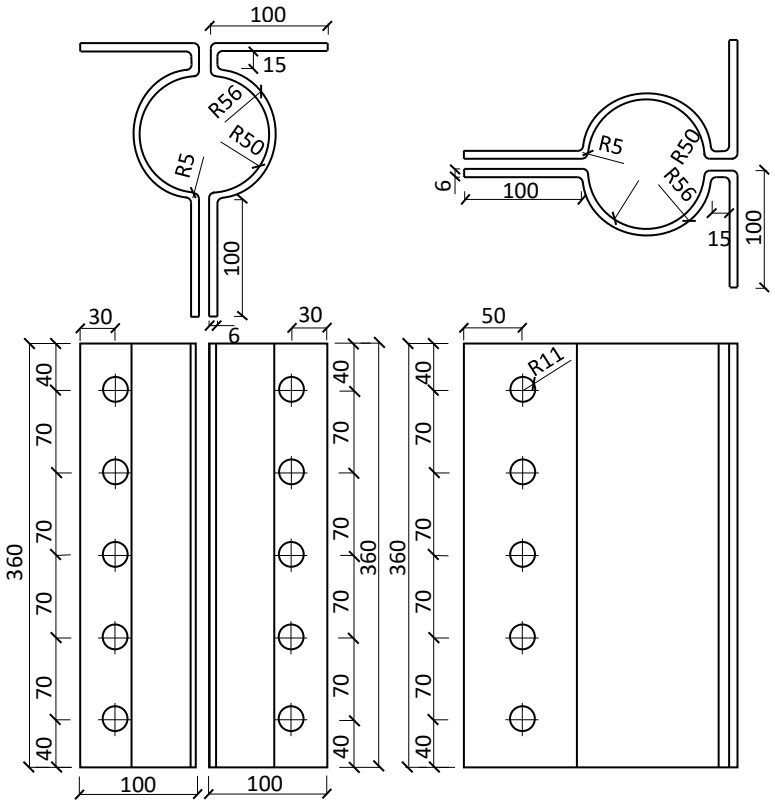

Figure 4. Dimensions of the connection for the case study.

3. DEVELOPMENT OF SIMPLIFIED ANALYTICAL MODELS

Any horizontal slice through the connection is mainly subjected to tensile and compressive forces which cause the semi-cylindrical section to bend. Plastic hinges will form in the cross-section where the maximum internal bending moments occur. Therefore, simple plastic

theory [29] is adopted to model the plastic behaviour of any slice through the cylindrical section. Material and geometric nonlinearities are considered. The effects of shear and axial forces on plastic moments are neglected, as they have very limited influence [30] on the formation and capacity of plastic hinges. According to the virtual work principle, the rate of work done by external loads should equal the rate of strain energy increase generated by the rotation of plastic hinges.

3.1. Calculation of the strain energy of a plastic hinge

A bi-linear stress-strain relationship is assumed at ambient temperature, changing to a tri-linear constitutive law for high temperature analysis, as shown in Figure 5(a).

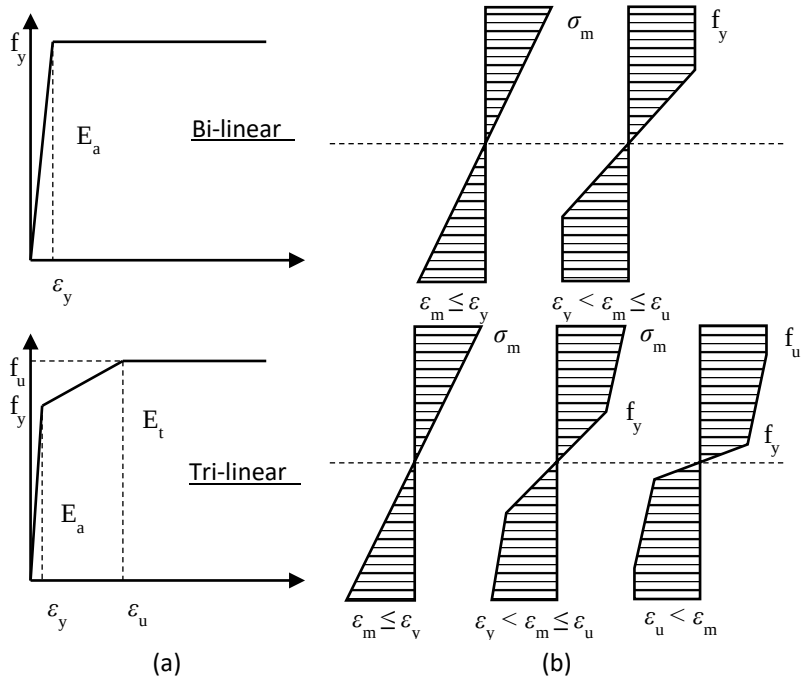

Figure 5. Material properties adopted; (a) Stress-strain relationships, (b) Stress distributions within the bending cross-section.

Yu's method [19] of calculating the strain energy of a plastic hinge is adopted. The derivation process is well documented, and so it is not described in detail here. The stress distributions

across the bending cross-section of a plastic hinge under different conditions are shown in Figure 5(b). The maximum strain is ε_m and the maximum stress within the cross-section is σ_m. The internal moment of the plastic hinge is calculated by integrating over the cross-section.

For the bi-linear stress-strain relationship:

When $\varepsilon_m \le \varepsilon_y$ $M_p = \frac{B_{eff} t^2}{2}\left(\frac{E\varepsilon_m}{3}\right)$ and $W_{PH} = B_{eff} t^2\left(\frac{1}{12} E\theta^2\right)$ (6)

When $\varepsilon_m > \varepsilon_y$ $M_p = \frac{B_{eff} t^2}{2}\left(\frac{E\varepsilon_y^3}{3\varepsilon_m^2} + \frac{f_y}{2}(1-\frac{\varepsilon_y^2}{\varepsilon_m^2})\right)$ (7)

and $W_{PH} = B_{eff} t^2\left(E\varepsilon_y^2 - 2f_y\varepsilon_y + \frac{6f_y\varepsilon_y^2 - 4E\varepsilon_y^3}{3\theta} + \frac{f_y\theta}{2}\right)$ (8)

For the tri-linear stress-strain relationship:

When $\varepsilon_m \le \varepsilon_y$, the equations are the same as for the bi-linear case.

When $\varepsilon_y < \varepsilon_m \le \varepsilon_u$ $M_p = \frac{B_{eff} t^2}{2}\left(\frac{E_t\varepsilon_m}{3} + \frac{(E-E_t)\varepsilon_y}{2} - \frac{(E-E_t)\varepsilon_y^3}{6\varepsilon_m^2}\right)$ (9)

and $W_{PH} = B_{eff} t^2\left\{\frac{E_t\theta^2}{12} + (E-E_t)\left(\frac{\theta\varepsilon_y}{2} + \frac{k^2\varepsilon_y^3}{6\theta} - \frac{k}{2}\varepsilon_y^2\right)\right\}$ (10)

When $\varepsilon_m > \varepsilon_u$ $M_p = \frac{B_{eff} t^2}{2}\left\{\frac{3\varepsilon_m^2 f_u + (E-E_t)(3\varepsilon_y\varepsilon_u^2 - \varepsilon_y^3) + 2E_t\varepsilon_u^3 - 3f_u\varepsilon_u^2}{6\varepsilon_m^2}\right\}$ (11)

and $W_{PH} = B_{eff} t^2\left\{\frac{E_t\varepsilon_u^2}{3} + (E-E_t)\left(\varepsilon_y\varepsilon_u - \varepsilon_y^2 + \frac{\varepsilon_y^3}{3\varepsilon_u}\right) + \Omega\left(\frac{k}{\varepsilon_u} - \frac{k^2}{\theta}\right) + \frac{f_u(\theta - k\varepsilon_u)}{2}\right\}$ (12)

in which $\Omega = (E-E_t)\left(\frac{\varepsilon_y\varepsilon_u^2}{2} - \frac{\varepsilon_y^3}{6}\right) + \frac{E_t\varepsilon_u^3}{3} - \frac{f_u\varepsilon_u^2}{2}$ (13)

where M_P is the plastic hinge moment capacity, W_{PH} is the strain energy, B_{eff} is the effective width of the cross-section and θ is the rotation angle of the hinge. If the length of

the plastic hinge is assumed to be equal to the thickness t of the cross-section, the rotation angle can be calculated as:

$$\theta=\int_0^t \frac{\varepsilon_m}{t/2}dx=2\varepsilon_m \tag{14}$$

3.2. Tensile analytical model

Since the proposed connection is symmetric, the analytical model is developed for half of the connection. Four plastic hinges, located at the two ends and the outer edge of the cylindrical section, are assumed to form during the deformation of the connection (Figure 6).

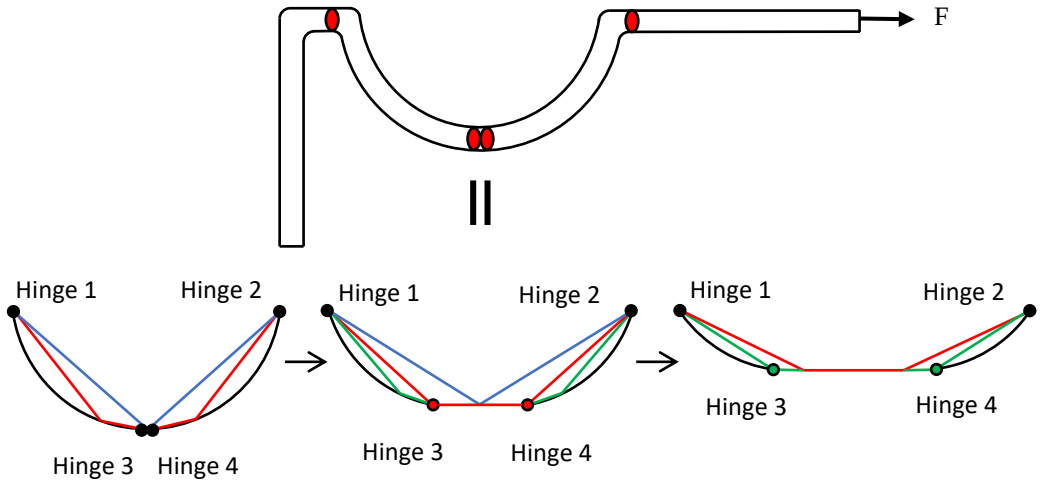

Figure 6. Location of plastic hinges in a deforming tensile mechanism.

Several assumptions are made for the tensile geometric model. As shown in Figure 6, the positions of the two end plastic hinges (Hinges 1 and 2) remain unchanged throughout the deformation process. However, the two hinges (Hinges 3 and 4) at the outer edges of the circular sections will move towards the end hinges as the section is stretched. During this process, the curvatures of the parts of the cross-section between Hinges 1 and 3 and between Hinges 2 and 4 remain unchanged. Finally, Hinges 3 and 4 respectively meet Hinges 1 and 2 when the cylindrical section has been stretched flat. Since the strain energy equations have

already been derived, the geometric relationship shown in Figure 7(a) between the displacement of the moving hinges and the rotation angle of each plastic hinge is the key to solving the virtual work equation.

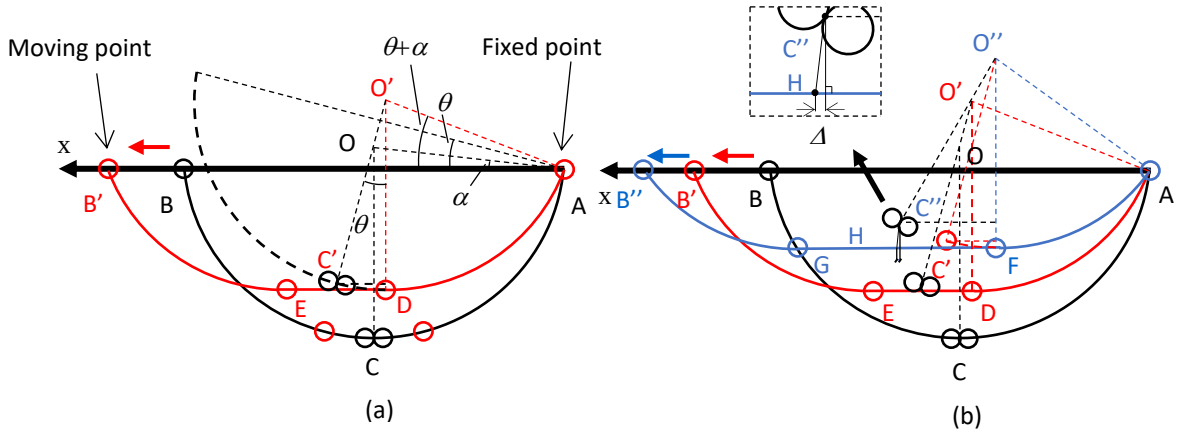

Figure 7. Geometric relationships in the tension model; (a) Geometric relationship, (b) Correction of displacement calculation.

The centre line of the semi-cylindrical cross-section is shown as OC in Figure 7. The black solid curve in the figure represents the original shape of the semi-cylindrical section. The red and blue solid lines represent the shapes of the cross-section at small and large deformations respectively. The angle of rotation about the plastic hinge of the arc centre relative to the x axis is α. It is assumed that the endpoint A of the arc is fixed, and the other end B moves along the x axis to deform the arc. It is obvious that the rotation angles of the four plastic hinges are always identical during the whole deformation process. When the plastic hinge at the fixed endpoint A rotates by a small angle θ (Figure 7 (a)), the black solid arc becomes the dashed arc. The new position of Hinge 4 should be the highest point on the dashed arc, which is the intersection point (D) of the vertical line (through the new centre point O') and the dashed arc. The new position of Hinge 3 should be at the mirrored position of Hinge 4 with respect to

Point C'. Thus, the displacement of the moving Point B is calculated as:

$$\Delta x = 2r\left[\sin\theta + \cos(\theta+\alpha) - \cos\alpha\right] \tag{15}$$

where r is the radius of the arc. Then, if there is a small rotation $d\theta$, the displacement increment of the moving point is:

$$dx = 2r\left[\cos\theta - \sin(\theta+\alpha)\right]d\theta \tag{16}$$

However, when the rotation angle of the plastic hinges is large, a displacement calculation error $\triangle$ occurs, shown as Figure 7(b). Point C is the centre-point between Hinges 3 and 4 in the initial state and Point H is the centre-point between Hinges 3 and 4 in the large-rotation stage. According to the geometric model assumption, the x-coordinate of Point C'' should be equal to that of Point H. However, as illustrated in the magnified part of Figure 7(b), this assumption is no longer true; there is a small horizontal distance $\triangle$ between Points C'' and H. The error $\triangle$ increases as the hinge rotates. Therefore, the originally calculated distance between Hinges 3 and 4 needs to be corrected. When the rotation angle θ is large, θ should be divided into n steps and the plastic hinge rotates by θ / n in each step. Accordingly, Equations (15) and (16) should be modified to：

$$\Delta x = 2r\left[n\sin\frac{\theta}{n} + \cos(\theta+\alpha) - \cos\alpha\right] \tag{17}$$

$$dx = 2r\left[\cos\frac{\theta}{n} - \sin(\theta+\alpha)\right] \tag{18}$$

According to the virtual work equation:

$$F dx = \int_0^{\theta+d\theta} 4M_p d\theta - \int_0^{\theta} 4M_p d\theta \tag{19}$$

Substituting Equations (6)-(14) and (18) into (19), the relationship between the external force F and the rotation of plastic hinge θ can be obtained.

For the bi-linear stress-strain relationship:

When $\varepsilon_m \le \varepsilon_y$ $$F = \frac{Eht^2\theta}{6r\left[\cos(\theta/n) - \sin(\theta+\alpha)\right]} \quad (20)$$

When $\varepsilon_m > \varepsilon_y$ $$F = \frac{ht^2\left[3\theta^2 f_y - \left(12 f_y\varepsilon_y^2 - 8E\varepsilon_y^3\right)\right]}{6\theta^2 r\left[\cos(\theta/n) - \sin(\theta+a)\right]} \quad (21)$$

For the tri-linear stress-strain relationship:

When $\varepsilon_m \le \varepsilon_y$, the equation is the same as that in the case of the bi-linear material.

When $\varepsilon_y < \varepsilon_m \le \varepsilon_u$ $$F = \frac{ht^2\left[E_t\theta^3 + (E - E_t)(3\theta^2\varepsilon_y - 4\varepsilon_y^3)\right]}{6\theta^2 r\left[\cos(\theta/n) - \sin(\theta+\alpha)\right]} \quad (22)$$

When $\varepsilon_m > \varepsilon_u$ $$F = \frac{ht^2\left[3\theta^2 f_u + (E - E_t)(3\varepsilon_y\varepsilon_u^2 - \varepsilon_y^3) + 2E_t\varepsilon_u^3 - 3 f_u\varepsilon_u^2\right]}{6\theta^2 r\left[\cos(\theta/n) - \sin(\theta+\alpha)\right]} \quad (23)$$

where h is the width of the connection and t is the thickness of the cross-section. A sensitivity analysis at ambient temperature is carried out to determine the appropriate value of n and the results are shown in Figure 8. Convergence is reached when n is larger than 10, and this value is therefore adopted.

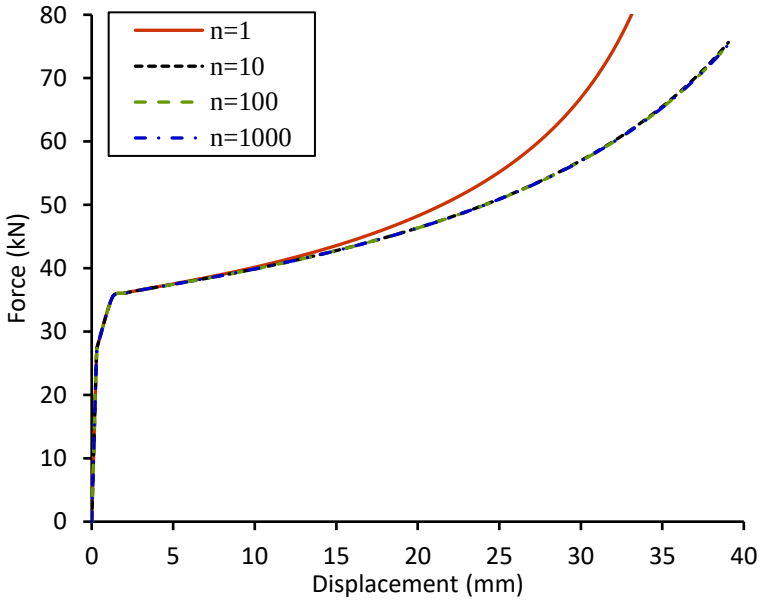

Figure 8. Influence of n value on tension curve.

3.3. Compressive analytical model

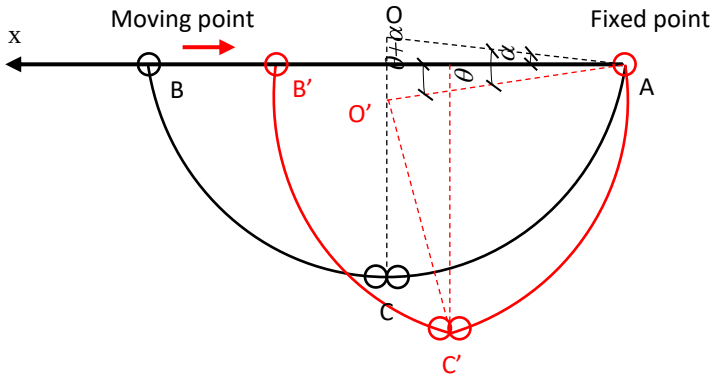

Figure 9. Geometric relationships of compression model.

The difference between the tensile and compressive models is that the positions of top two hinges (Hinges 3 and 4) remain unchanged in the compressive model. According to the geometric relationships shown in Figure 9, the calculation equation for displacement should be:

$$\Delta x = 2r[\cos\alpha - (\cos(\theta-\alpha) - \sin\theta)] \tag{24}$$

Then, if there is a small rotation $d\theta$, the displacement increment is:

$$dx = 2r\left[\sin(\theta-\alpha) + \cos\theta\right]d\theta \tag{25}$$

Substituting Equations (6)-(14) and (25) into (19), the relationship between external force F and the rotation angle θ of the plastic hinge can be obtained:

For the bi-linear stress-strain relationship:

When $\varepsilon_m \le \varepsilon_y$ $$F = \frac{Eht^2\theta}{6r\left[\sin(\theta-\alpha)+\cos\theta\right]} \tag{26}$$

When $\varepsilon_m > \varepsilon_y$ $$F = \frac{ht^2\left[3\theta^2 f_y - \left(12 f_y\varepsilon_y^2 - 8E\varepsilon_y^3\right)\right]}{6\theta^2 r\left[\sin(\theta-\alpha)+\cos\theta\right]} \tag{27}$$

For the tri-linear stress-strain relationship:

When $\varepsilon_m \le \varepsilon_y$, the equation is the same as that in the case of bi-linear material.

When $\varepsilon_y < \varepsilon_m \le \varepsilon_u$ $$F = \frac{ht^2\left[E_t\theta^3 + (E - E_t)(3\theta^2\varepsilon_y - 4\varepsilon_y^3)\right]}{6\theta^2 r\left[\sin(\theta - \alpha) + \cos\theta\right]} \quad (28)$$

When $\varepsilon_m > \varepsilon_u$ $$F = \frac{ht^2\left[3\theta^2 f_u + (E - E_t)(3\varepsilon_y\varepsilon_u^2 - \varepsilon_y^3) + 2E_t\varepsilon_u^3 - 3f_u\varepsilon_u^2\right]}{6\theta^2 r\left[\sin(\theta - \alpha) + \cos\theta\right]} \quad (29)$$

3.4. Push-pull behaviour of a connection

Applying Equations (20)-(23) and Equations (26)-(29) for a connection of depth 360 mm and plate thickness 6mm with a semi-circular inner radius 50 mm, fabricated in steel of grade S275, a continuous curve linking force and movement can be constructed, and this is shown in Figure 10. It can be seen that the tensile curve stiffens with displacement after its plastic mechanism has been created, while the compressive curve reduces its force with displacement, at least until it is fully compressed when the two edges contact one another.

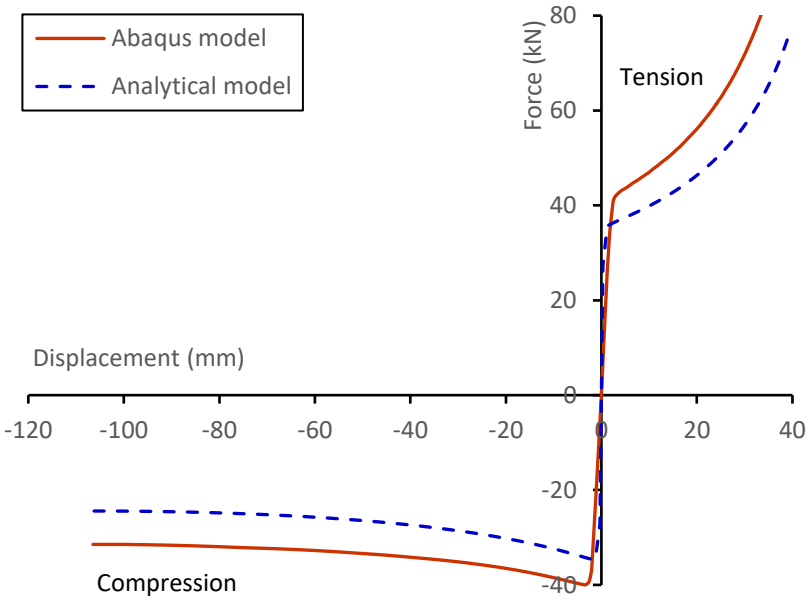

Figure 10. Full push-pull force-displacement curve for the example connection strip.

3.5. Rotational model

The concept of the component-based method can be used here to model the rotational

behaviour of the whole connection using a set of identical connection strips as parallel components. As can be seen in Figure 11, the whole connection is divided into a number of horizontal strips.

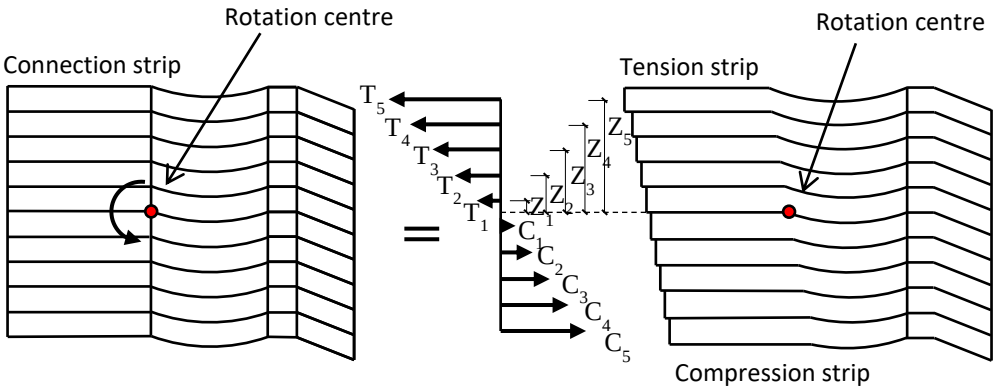

Figure 11. Rotational connection strip component-based model.

When the connection is rotated about its centre point, these strips are either pushed or pulled. The normal force of each strip under tension or compression can be calculated using the tension or compression models described previously. Then the rotational moment of the whole connection can be obtained by calculating the moment of each strip's force about the centre of rotation:

$$\mathrm{M} = \sum_{\mathrm{i}=1}^{\mathrm{N}/2} (\mathrm{T_i} + \mathrm{C_i}) \mathrm{Z_i} \tag{30}$$

In this equation N is the total number of connection strips and $\mathrm{Z_i}$ is the distance between the centre point of the i th connection strip and the centre of rotation of the entire connection. A sensitivity analysis was carried out at ambient temperature to find the appropriate strip number N, and the results are shown in Figure 12.

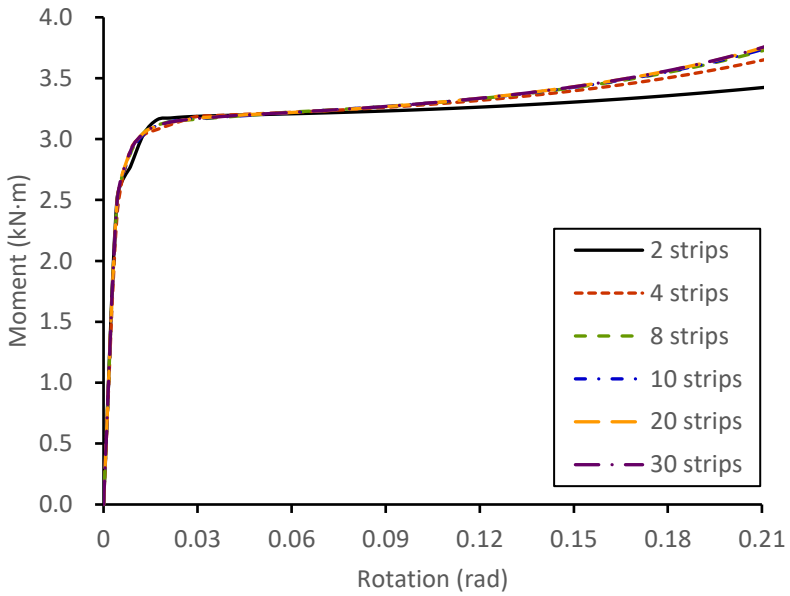

Figure 12. Influence of total number of strips on connection moment.

It can be seen that the resulting curve of the analytical model with 8 connection strips is consistent enough, but the connection models at high temperatures have adopted 10 strips. However, it has been seen from Figure 10 that the tensile strength of the connection is higher than its compressive strength in the plastic stage. Under the same displacement, a tension connection strip will generate a larger force than the corresponding compression strip. Therefore, an external axial force, which may be the reaction at the centre of rotation, is required to equilibrate this model. A model to which a pure moment is applied will experience a shift of its centre of rotation in order to balance the total tension and compression forces; this will be accompanied by a horizontal movement of the centre of rotation.

4. VALIDATION OF ANALYTICAL MODELS AGAINST ABAQUS FE SIMULATION

In this section, the general-purpose finite element software Abaqus is used to validate the tensile, compressive and rotational analytical models proposed, at both ambient and elevated temperatures. The shell element S4R is adopted in the Abaqus simulation, to save cost in

computation compared with the use of solid elements.

4.1. Validation of tension and compression models at ambient temperature

The geometries of the tension and compression models are identical, and the details are those shown in Figure 4. The material used is S275 steel. As for the boundary conditions of the Abaqus model, the end-plate is fixed and the out-of-plane displacement of the fin-plate is constrained by being bolted to the beam web. A mesh sensitivity analysis indicated that an element size of 10mm x 10mm was adequate for the connection model.

The analytical model is in satisfactory, although not complete, agreement with the Abaqus model; the comparison of two models is shown in Figure 10. The initial slopes of the tension and compression curves in the linear-elastic stage are equal. In the plastic stage, as the connection is pulled in tension, the force required increases steadily up to the tension deformation limit is reached, when the connection is effectively straightened, and the four plastic hinges are located on the same line. The slope of the tension curve in the plastic stage increases continuously and becomes almost vertical near to the tension deformation limit, because of the continuous reduction of the lever arm between the applied axial force and the top two plastic hinges (Hinges 3 and 4 in Figure 6). For the compression curve, the force required to increase the compression displacement decreases steadily in the plastic stage up to the final compression deformation limit, at which contact, either within the cylindrical section or between the cylindrical section and the end-plate, occurs. This is opposite to the trend of the tension curve due to the increasing lever arm between the applied force and the top two plastic hinges.

4.2. Validation of rotation model at ambient temperature

For the analytical rotational model, the connection behaviour is considered as the sum of its components' behaviour. Rotation of the entire connection is simulated by tension and compression of each connection strip. Deformation compatibility of two adjacent connection strips is only piecewise in this analytical model; this ignores the horizontal shear force between adjacent strips. In order to make a more reasonable comparison between the analytical and Abaqus models, two Abaqus connection models were created, which are shown in Figure 13. These were used to study the effect of the shear between strips on the rotational behaviour of the whole connection. In the strip model compatibility is maintained between adjacent strips except with respect to horizontal movements, although the ends of each strip are tied so that their movements are in a straight line. As with the component-based analytical model, defined in Figure 11, the connection is constrained to rotate about a point at the base of the fin-plate, about which it is also free to move in the vertical direction, although restrained in the axial direction.

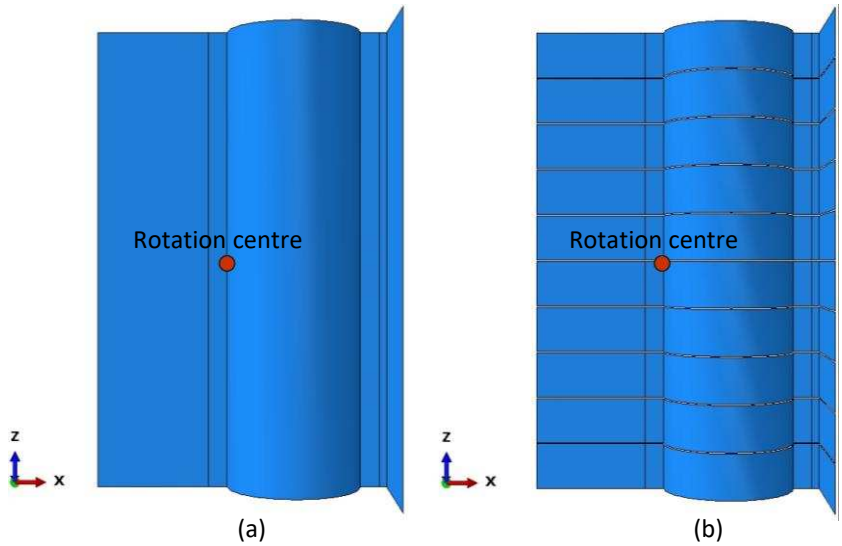

(a) (b)

Figure 13. Two Abaqus models; (a) the whole connection piece, (b) the strip model.

The comparison of the two Abaqus models and the analytical model is shown in Figure 14. A significant difference can be seen between results from the Abaqus strip model and the analytical model. The difference between the Abaqus strip model and whole connection model indicates that an additional moment is generated by the shear force between adjacent strips in providing rotation compatibility, mainly due to compatibility of the torsional rotations of adjacent strips. This compatibility is hard to implement in a simple model and it is considered unnecessary to include it; this might be considered using a safety factor at a later stage. The discrepancy between the Abaqus strip model and analytical model will be explained later in Section 4.4. In any case, the analytical model gives a more conservative result than either Abaqus model.

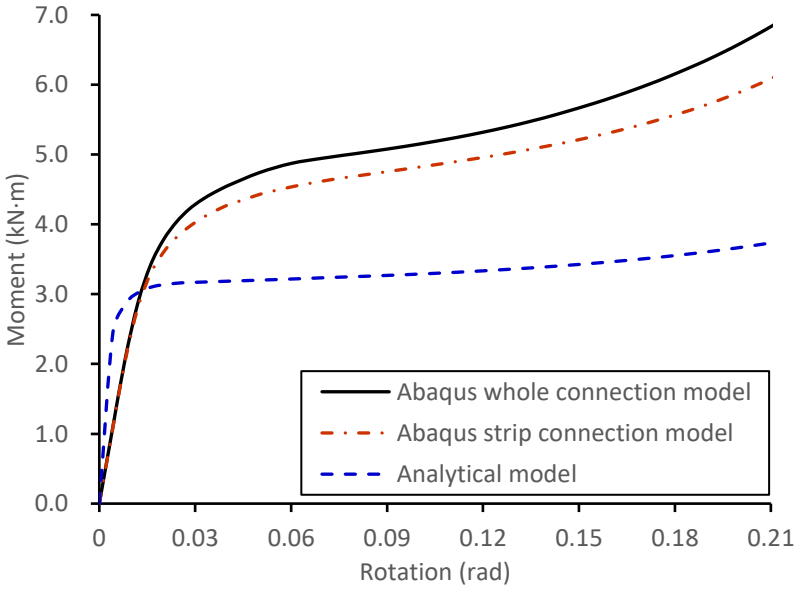

Figure 14. Comparison of rotation analytical model against Abaqus models.

4.3. Validation of analytical models at elevated temperatures

The material properties of the connection at elevated temperatures are calculated according to Eurocode 3 Part 1-2 [31]. For Abaqus simulation, the model is first heated to a pre-defined

temperature and then a pure tension, compression or rotation displacement is applied to the model to obtain the force-displacement curve under at this temperature value. The comparison of the Abaqus and analytical models over a range of elevated temperatures is shown in Figure 15 and Figure 16.

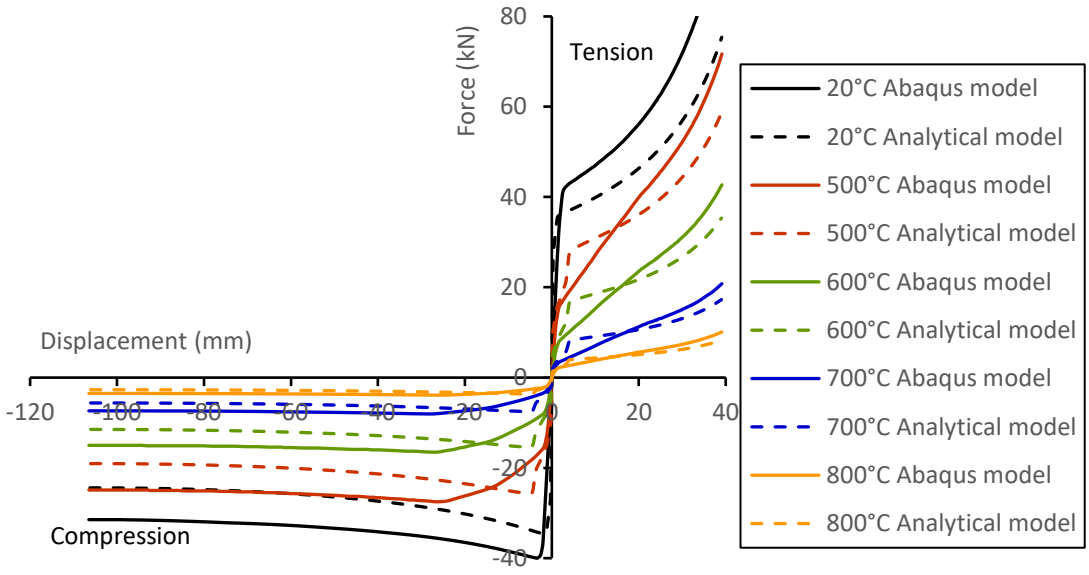

Figure 15.Comparison of tension/compression analytical push-pull model against Abaqus model at elevated temperatures.

It can be seen from Figure 15 and Figure 16 that all curves are of the same shape, and the difference between analytical and Abaqus models decreases as temperature rises. This indicates that temperature does not influence the deformation mode of the connection. Above 400°C the force required to produce a certain deformation decreases progressively with increase of temperature. However, it is obvious that this novel connection can provide satisfactory push-pull ductility at elevated temperatures.

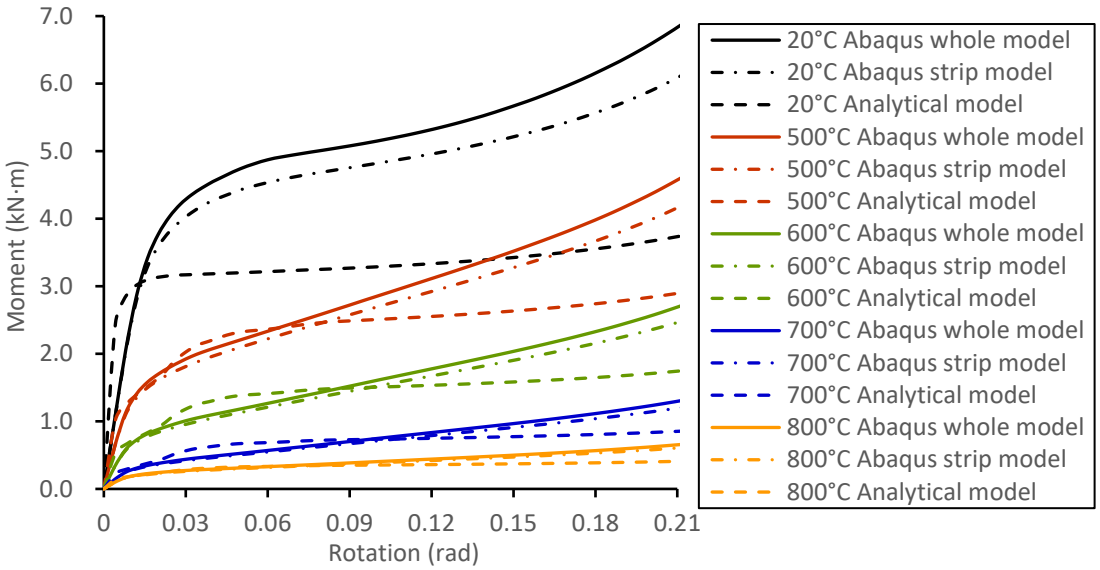

Figure 16. Comparison of rotational analytical model against Abaqus model at elevated temperatures.

As mentioned above, with a fixed centre of rotation the force equilibrium of the rotational model is not satisfied due to the difference between the resultant forces in the tensile and compressive zones of the connection. Therefore, external axial reaction forces are required to balance the model of the connection during the rotation process at different temperatures; these axial forces, obtained by the analytical and Abaqus models are shown in Figure 17

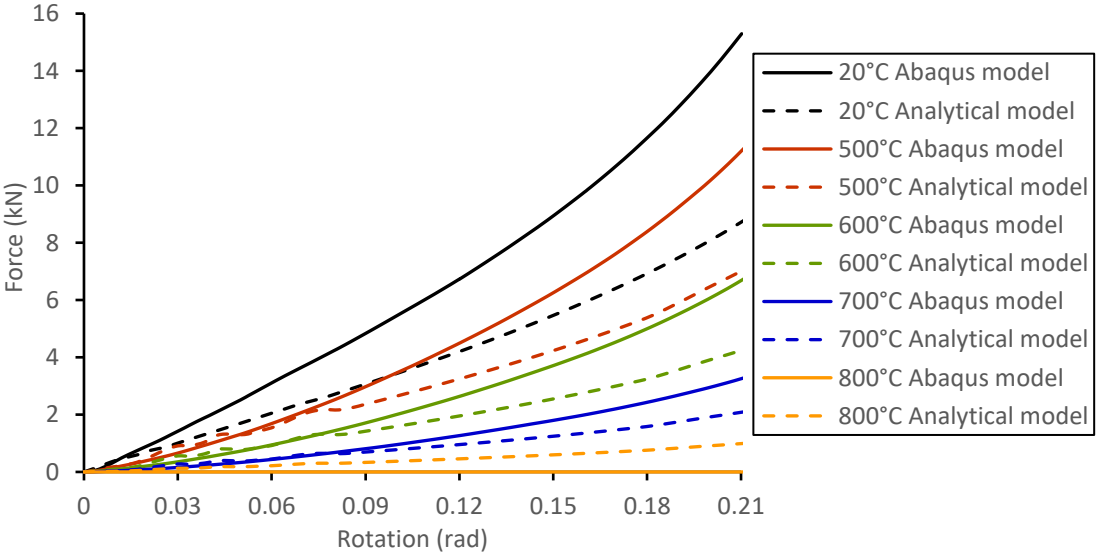

Figure 17. Resultant axial forces of the connection during rotation.

4.4. Analysis of the discrepancy between analytical and Abaqus models

Differences can be seen between the tension/compression analytical model and the Abaqus model in Figure 10 and Figure 15. In the initial elastic stage, the analytical model is stiffer than the Abaqus model, which is reasonable due to the simplifications in this phase of the analytical model. For example, the elongation of the connection's cross-section is not considered in the analytical model. Therefore, the deformation of the Abaqus model under any load level is slightly greater than that of the analytical model. In the plastic stage, the Abaqus model becomes the stronger of the two because of the positions of the plastic hinges. In the analytical model It is assumed that a plastic hinge is generated at a discrete point. However, it can be seen from Figure 18 and Figure 19 that the end plastic hinge of the Abaqus model is not located at a precise point but has a finite length, which gradually increases and then stabilizes at a certain value as the deformation of the connection proceeds. As described above in the derivation of the analytical model, the position of the plastic hinge is related to the variable α. The change of length of the end plastic hinge in the Abaqus model could be explained as being equivalent to an analytical model with a different initial angle α. Larger plastic hinge lengths cause greater values of the variable angle α.

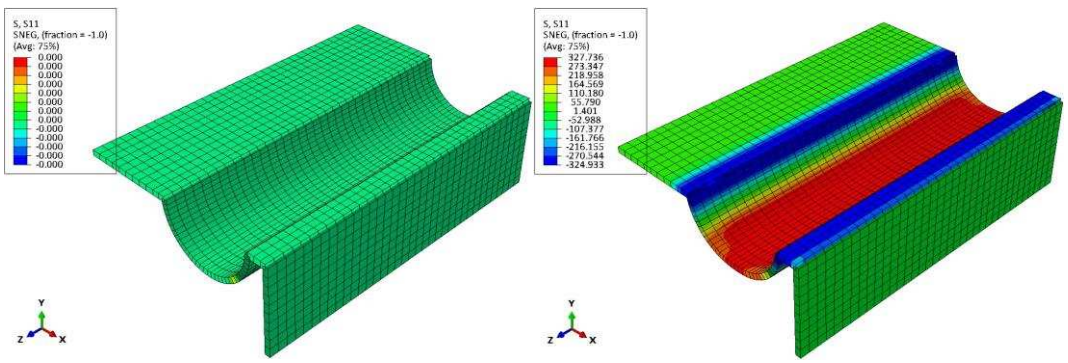

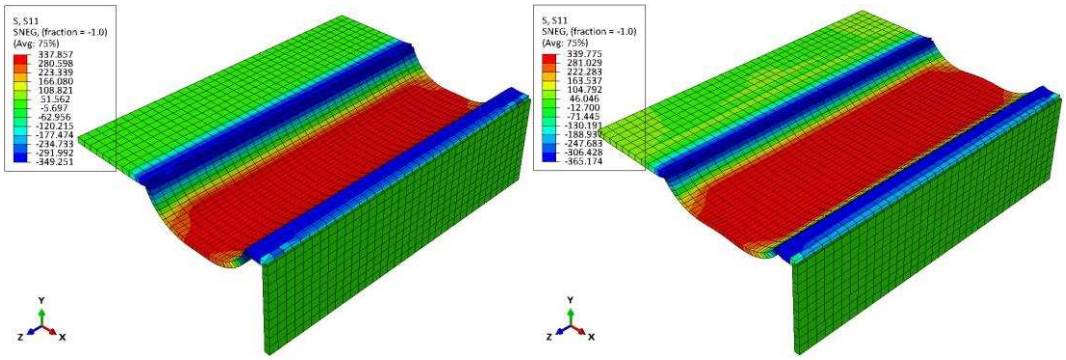

Figure 18. Stress distribution of Abaqus tension model.

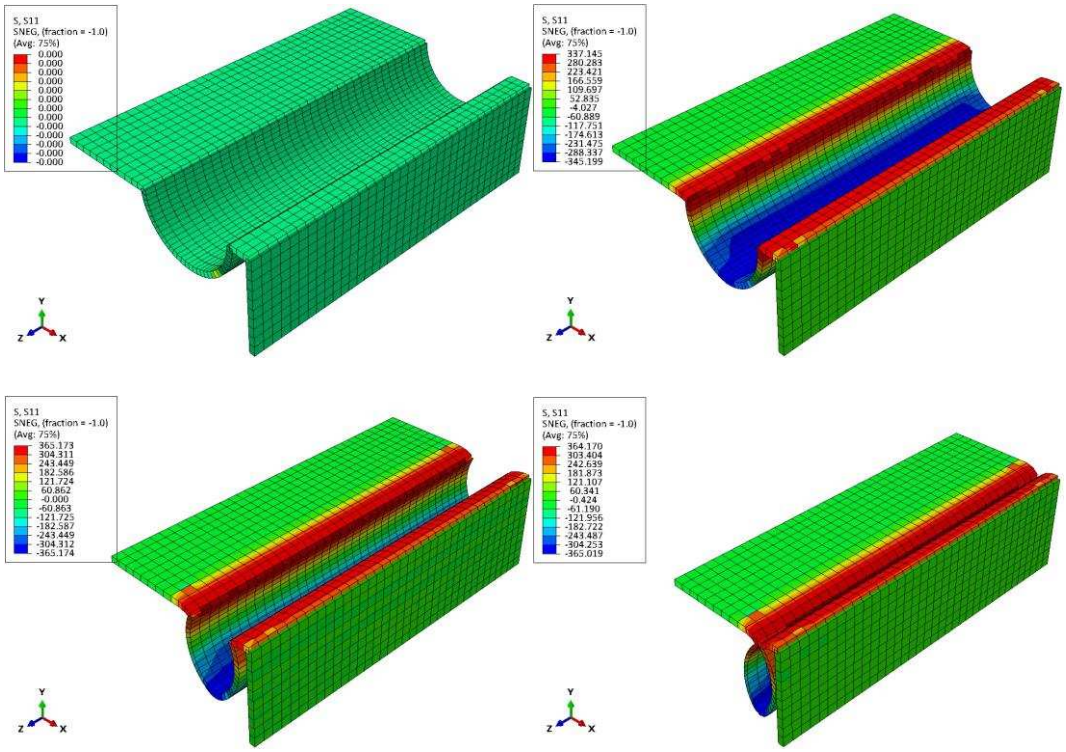

Figure 19. Stress distribution of Abaqus compression model.

In the tension case, the displacement of the Abaqus model in the plastic stage is slightly lower than that of the analytical model at a certain force value, because the part of the deformed shape that is straight and parallel to the force direction in the analytical model (between Hinges 3 and 4 in Figure 6) has some reverse curvature, as shown in Figure 20.

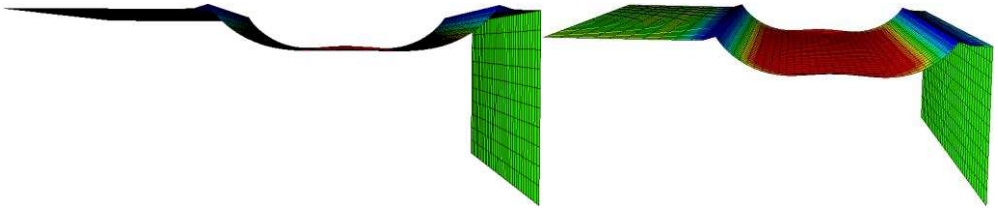

Figure 20. Reverse curvature between the two intermediate plastic hinges in tension.

The discrepancy between the rotational mechanical and Abaqus models is significant, as has been shown in Figure 14 and Figure 16. The main reason for this discrepancy seems to be that compatibility of the torsional rotations of the parts of the semi-circular connection strips which are more aligned perpendicular to the fin-plate has been ignored in the mechanical model. As shown in Figure 21(a), the rotational behaviour of the entire connection consists of two actions, namely tension/compression and torsion/bending of each connection strip. The variation of in-plane moment at the end of every strip is shown in Figure 21(b), and the sum of these moments is shown in Figure 22 (the blue curve).

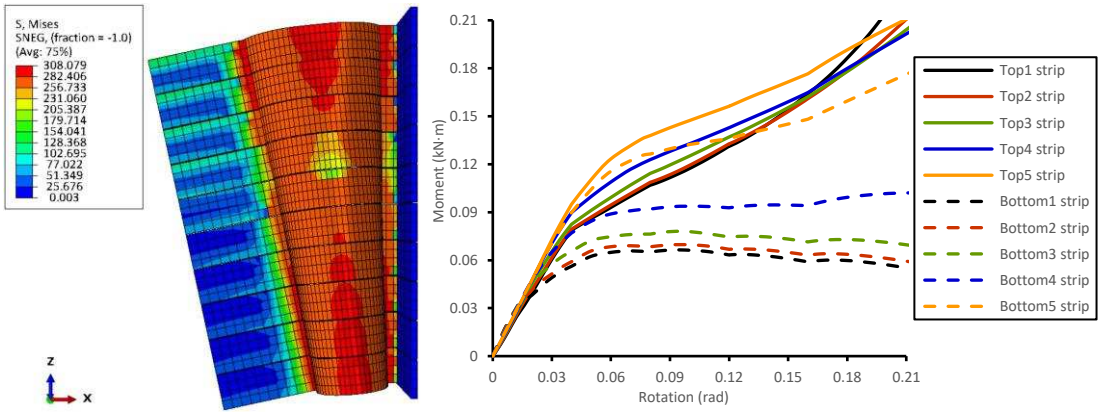

(a) (b)

Figure 21. Bending of connection strips; (a) Deformed shape of Abaqus strip model, (b) End moments of connection strips.

The red curve shown in Figure 22 is obtained by subtracting the analytical model curve in Figure 14 from the Abaqus curve. Its initial value is negative, due to the fact that the analytical model is stiffer than the Abaqus model in the initial elastic stage. It can be seen from Figure

22 that the sum of the strips' end moments is very close to the difference between the analytical and Abaqus model, which indicates that bending/torsion of strips is the main cause of the difference. In order to illustrate this difference more clearly, the sum of the strips' end moments, shown in Figure 22(b), is added to the original analytical model's curve from Figure 14 to form a modified analytical model curve, shown in Figure 23. As can be seen from this figure, the modified curve is very close to the Abaqus strip model curve.

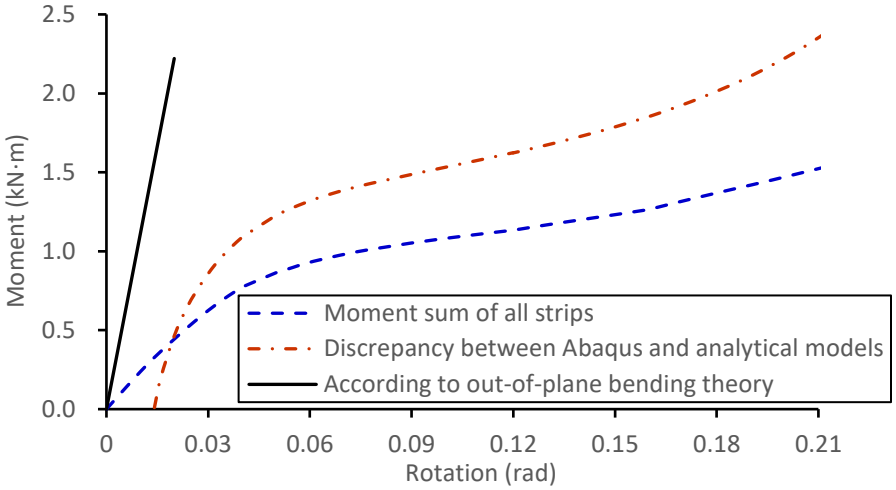

Figure 22. Analysis of discrepancy between rotation analytical model and Abaqus model.

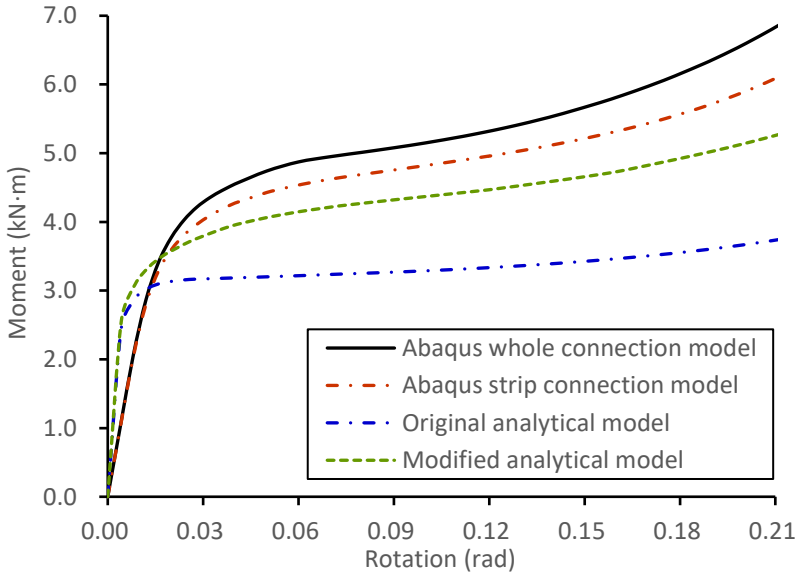

Figure 23. Modified rotational analytical model curve.

The in-plane bending behaviour of a circular ring has been well studied in the past [32, 33]. As for out-of-plane bending behaviour, Krahula [34] proposed a calculation method; the relationship between moment and rotation angle is described as:

$$\begin{aligned} \mathrm{r}\varphi = &-\mathrm{A}\sin\phi - \mathrm{B}\cos\phi + \mathrm{C}\alpha\cosh\sqrt{\alpha}\phi + \mathrm{E}\alpha\sinh\sqrt{\alpha}\phi + \mathrm{H}\sin\phi + \frac{4\kappa\mathrm{H}}{\mathrm{M}}\cos\phi \\ &- \mathrm{H}\left[\frac{(\alpha+\beta+1)}{2(\alpha+1)}(\phi\cos\phi + 2\sin\phi) + \frac{2\kappa}{\mathrm{M}}\frac{(\alpha+\beta+1)}{(\alpha+1)}(-\phi\sin\phi + 2\cos\phi)\right] \end{aligned} \tag{31}$$

Where r is the radius of the ring, φ is the out-of-plane rotation angle, M is the out-of-plane moment, ϕ is the angular coordinate of the cross-section of the ring. The calculation equations for constant α, β and H are documented by Krahula, and are not described here. A, B, C, E, F and κ are six constants determined by the boundary conditions of the circular ring. However, the relationship between angle and moment given by (31) is linear-elastic. The black line in Figure 22 is calculated by this method, and the slope of this line is very close to the slope of the red line in the elastic stage. However, it is very difficult to study the bending and torsion behaviour of a connection strip by a theoretical method. Each connection strip is pushed or pulled at the same time as it is bent and twisted. This means that the cylindrical section will no longer remain circular in shape, and circular ring bending theory is no longer appropriate. The boundary conditions of the cylindrical section are hard to describe. There is a small curved section between the cylindrical section and the end-plate, so that the boundary conditions of the cylindrical section at this end cannot be simply treated as fixed-ended or simply-supported. In the context of the moment necessary to apply a significant rotation to the beam-end, the moment generated by applying the same rotation to the connection is small, and so an exact model of aspects such as bending and twisting of connection strips is

not very important to this study.

5. VALIDATION OF THE ANALYTICAL MODELS AGAINST EXPERIMENTS

Experiments on this novel connection have been carried out at model scale by Kalawadwala [35]. In this section the experiments conducted by Kalawadwala are used to test the tension/compression analytical model at ambient temperature.

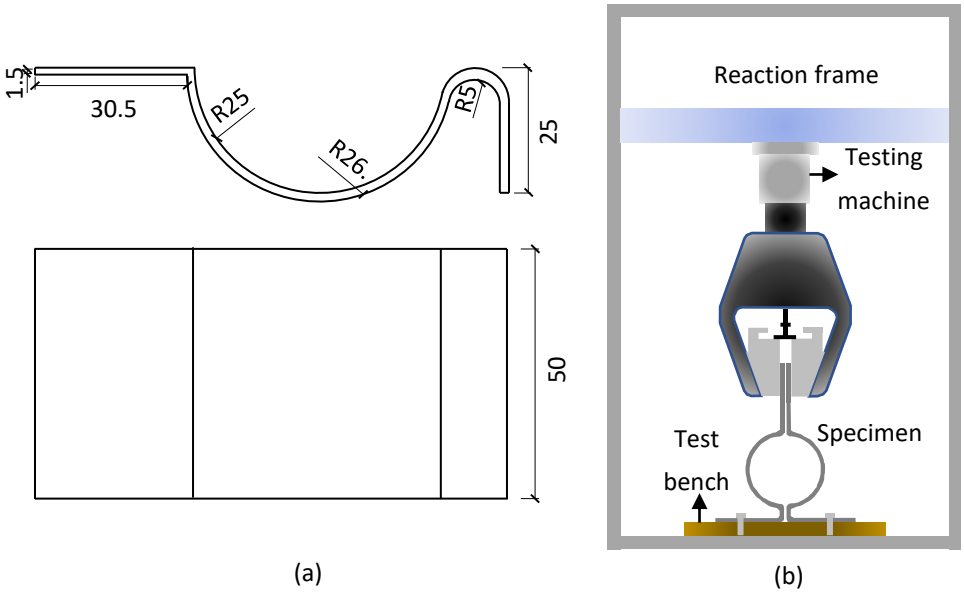

Figure 24. Test setup and specimen dimensions; (a) Dimensions of the ambient-temperature test specimens, (b) Test setup.

S275 steel was used by Kalawadwala to produce the test specimens. The dimensions of the specimens are shown in Figure 24(a); the test setup of the ambient temperature tests, shown in Figure 24(b), used a 10 kN Shimadzu universal testing machine to apply compressive axial force to the specimen. The force was measured by a load cell. The deformation of the connection specimens during tension and compression tests is shown in Figure 25, and the comparison between the analytical model and experiments is shown in Figure 26.

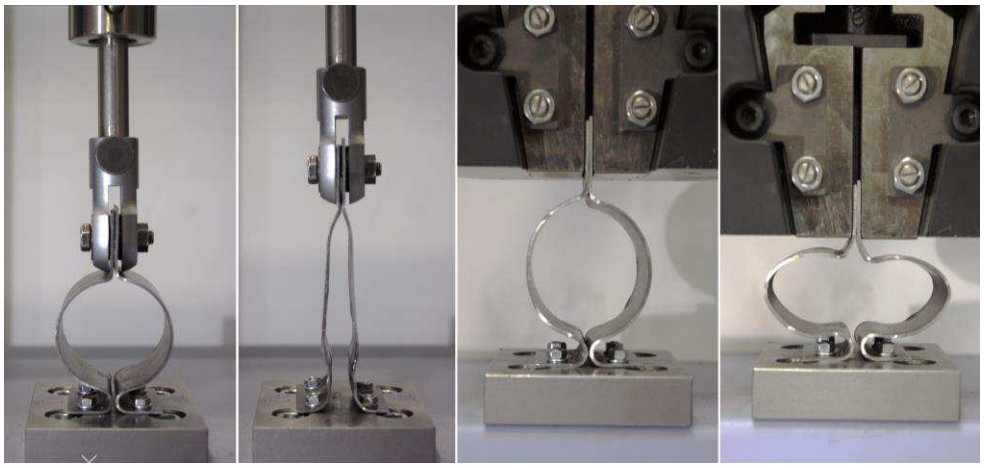

(a) (b)

Figure 25. Deformation of connection during tests: (a) Tension test, (b) Compression test.

As shown in Figure 26, the initial stiffnesses of the analytical curves are higher than that of the experimental curves. A potential reason for this is that both the cylindrical section and the low-radius curved section between the cylindrical section and the end-plate contribute to the total displacement during the whole loading process, whereas only the cylindrical section is considered in the analytical models. This simplification was made on the basis that the connection ductility at large deformation phase and the ultimate strength are perhaps more important than the initial elastic stiffness for structural fire engineering analysis, where the prevention of fracture/collapse is the key concern. A satisfactory correlation was obtained in tension between the experimental and analytical model curves. In compression, the test specimen behaved in a stronger manner, requiring higher force to generate displacement than the analytical model. A potential reason for this is that contact could occur at high deformation between the cylindrical section and the test-bench bolt, as shown in Figure 25 (b). This could also enhance the compressive strength of the connection test specimen. These factors have not been considered in the analytical model. However, the general trend of the experimental

and analytical curves shows good correlation in both the tension and compression quadrants.

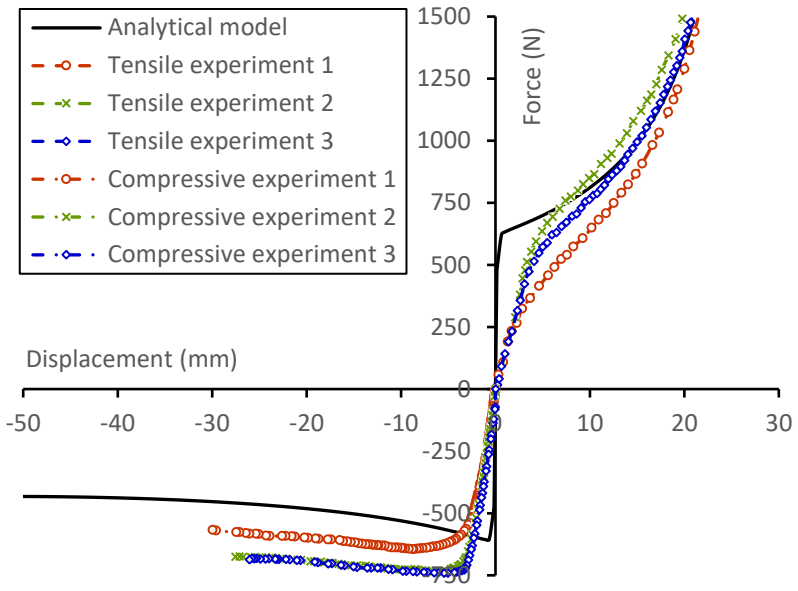

Figure 26. Comparison of analytical model against experiment at ambient temperature.

6. CASE STUDY FOR THE NOVEL CONNECTION

After the development of the novel connection and its analytical models, which have been described above, a preliminary study is now conducted on the performance of the new connection in a structural subframe. An isolated 7.5m beam of UKB 533x210x109 section with an appropriately designed novel connection at its ends is investigated here; the dimensions of the connection are the same as those shown in Figure 4.

Simplifications of the FEM model, as shown in Figure 27, are listed as follows:

- One half of the model is created to save computational cost, and an axis of symmetry is applied as a boundary at mid-span of the beam.
- The complex contact conditions between bolts and clearance holes lead to non-convergence of the simulation using a static solver, and therefore are not considered in this preliminary study. To avoid complex contacts within the connection zone, the bolts

are not modelled, and the fin-plate is directly tied to the corresponding area of the beam web.

- Constraint boundary conditions are applied at the bolt positions of the end-plate, connecting it to a fixed thick plate representing the column flange.
- Simple hard contacts are defined between the fin-plate and beam web, and between the end-plate and column flange.

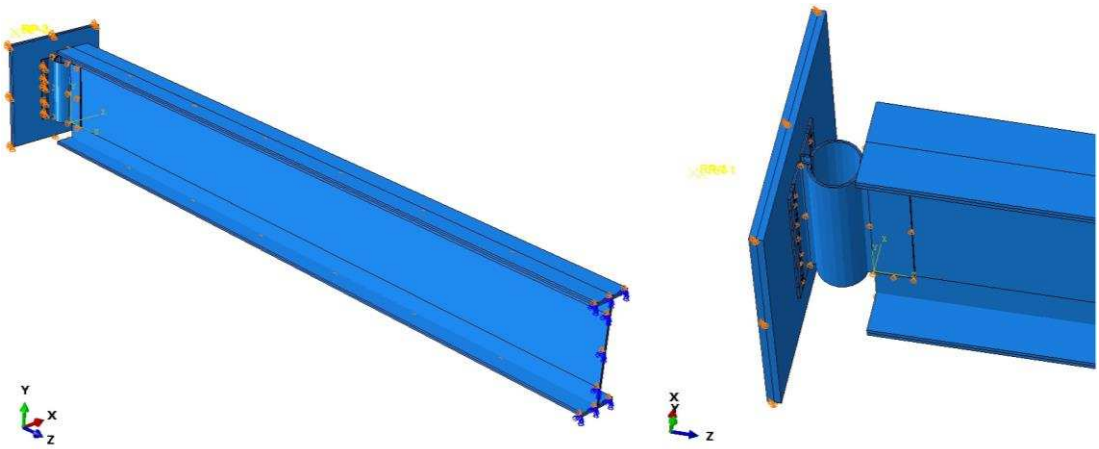

Figure 27. Abaqus model of beam with ductile connection.

The element size in the connection model is similar to that used in the half connection model presented in chapter 4. Since the behaviour of the connected beam is not the prime concern of the simulation, its mesh size can be much coarser than that of the connection, to save computational time. External load is first applied to the beam flange at ambient temperature, generating a load ratio of 0.31 with respect to a simply supported beam and then the temperature of the model is gradually increased until the simulation fails to converge. It should be noted that 0.31 is a relatively low load ratio in practical terms. This example serves as a case study in this paper. Future parametric studies have been planned to investigate the performance of the novel connection subject to different load ratios. The results will

contribute to the development of the practical design guidance of the novel connection. It is assumed that the temperature distribution within the beam and connection is uniform across the depth. Lawson [5, 6] assumed that the temperature of the connection was about 70% of that of the bottom flange at the mid-span of the beam. In order to study the effect of temperature on analytical behaviour of the connection, two cases are simulated, in which the connection temperature is set to 70% and 100% of the beam temperature respectively. The deformation of the connection during the entire simulation process is shown in Figure 28. It can be seen that the cylindrical section is initially squeezed due to thermal expansion of the connected beam at temperatures up to about 600°C, beyond which the beam develops catenary action, and the rotation angle of the connection increases rapidly with the increase of beam deflection. Eventually, large strains are formed around the top of the cylindrical section, and the connection starts to fail. It can be concluded that the novel connection can accommodate large deformations induced by the connected beam because the ductility of its cylindrical section allows the fin-plate to move towards and away from the end-plate.

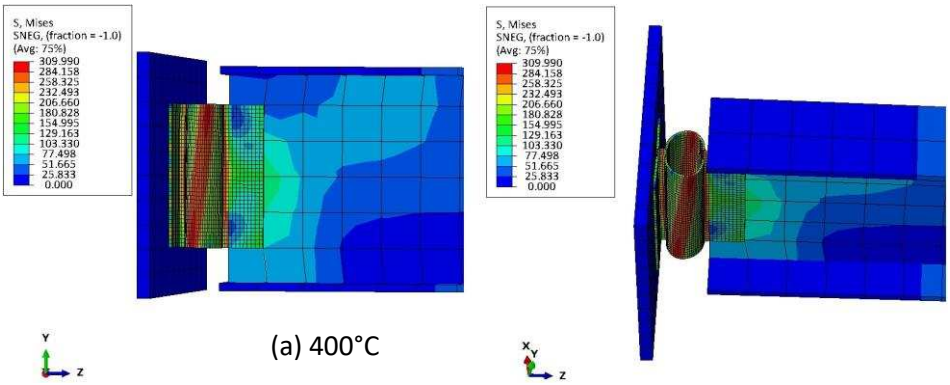

(a) 400°C

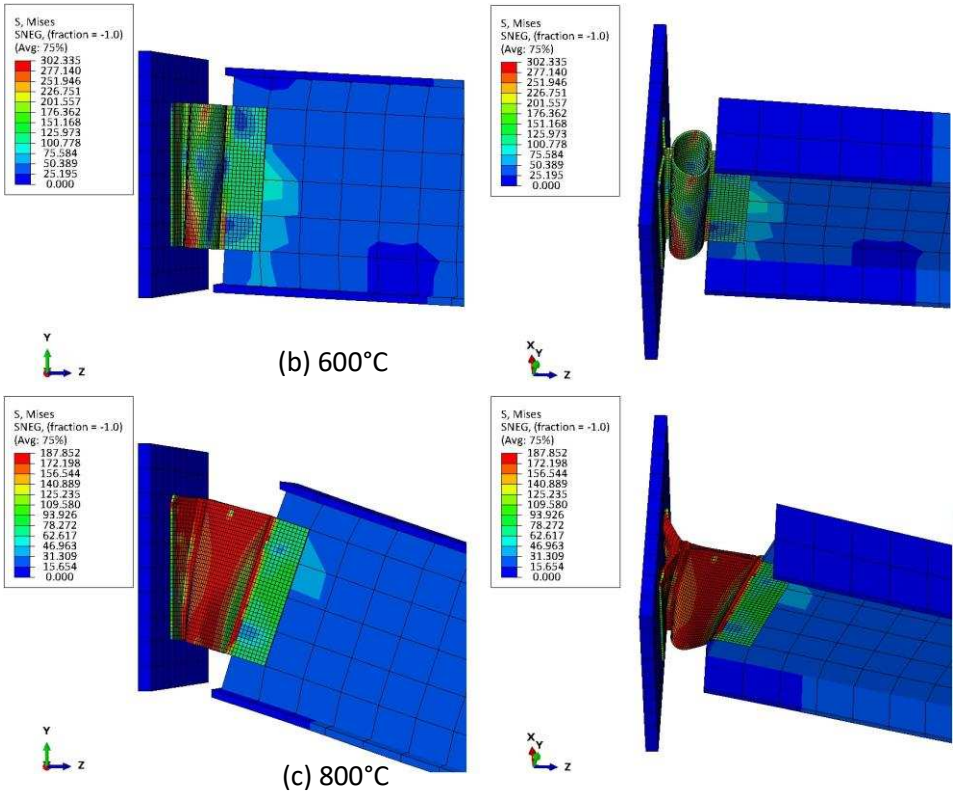

Figure 28. Deformation of the connection ($T_C = 70\%T_B$).

Deflections of the mid-span of beams with different boundary conditions are shown in Figure 29. It can be seen that curves representing the novel connection are very close to the dashed curve representing the case with simply supported boundaries. The comparison of axial forces (Figure 30) shows that the axial force generated in the beam with the novel connection is significantly reduced due to the high axial ductility created. Thus, the conclusion can be tentatively drawn that the novel connection behaves more like an idealized pinned joint and has considerable axial ductility to accommodate the deformation of the connected beam in reducing axial forces. This novel connection will be implemented within Vulcan, and then its ability to reduce the axial force of connected beam will be verified against the Vulcan model. In the cases where the connection temperature is 70% of the beam temperature, the beam deflects more than when the connection temperature is equal to the full beam temperature.

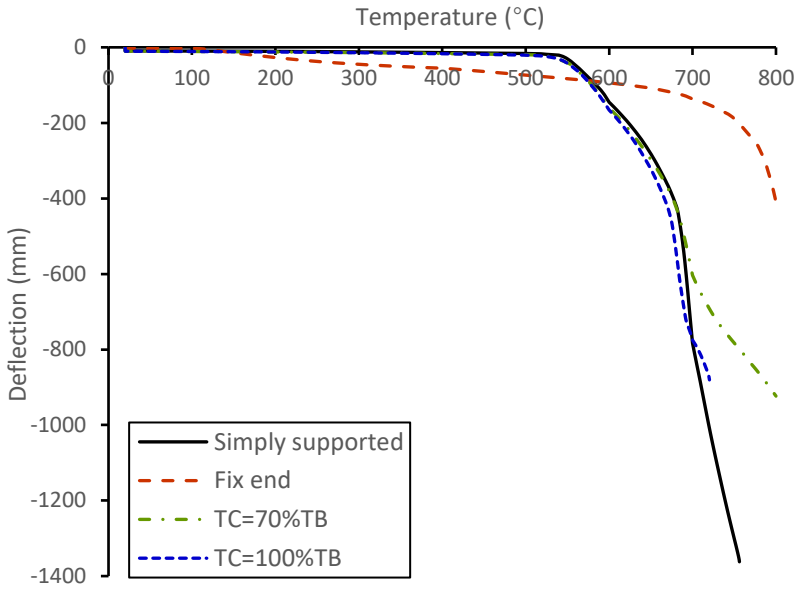

Figure 29. Deflection at the beam mid-span.

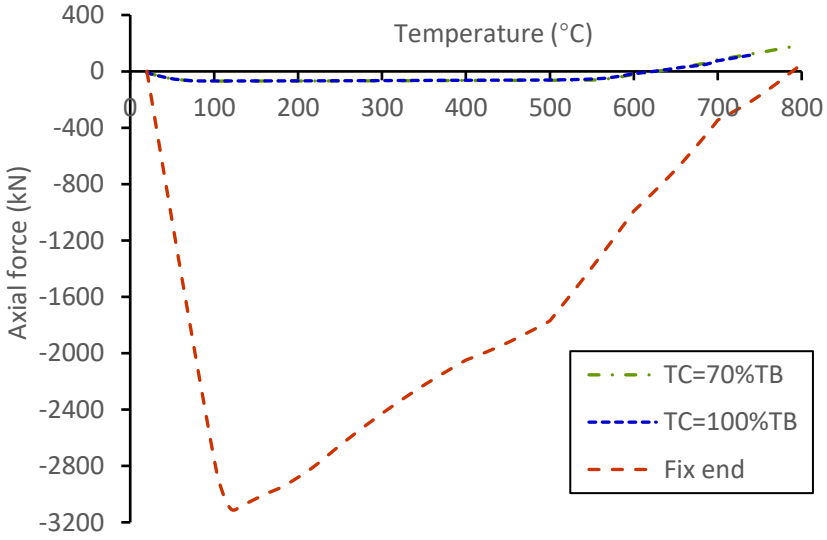

Figure 30. Comparison of beam axial forces.

To assess the influence of the beam span on the performance of the novel connection, four different beam spans are adopted. The corresponding beam sections are listed in Table 1. Except for the connection depth, the other dimensions of the connections (e.g. plate thickness and cylindrical section radius) are the same in all four cases. The comparative results are show in Figure 31 and Figure 32, which illustrate the connection rotation and the axial forces generated in the beams of different spans. It can be seen from Figure 31 that the novel

connection can rotate a significant angle before failure occurs, which once again demonstrates its good deformability. Figure 32 shows that with the increase of beam span, the beam axial force also increases. Reason leads to this may be that the radius of cylindrical section, which is the most critical factor affecting the connection ductility, is insufficient in the case of the relatively long-span beam. Further studies are required to establish guidance on the optimum radius of cylindrical section. In general, the novel connection can be regarded as a ductile connection and can provide satisfactory deformation capacity.

Table 1. Parameters of the beams of various spans.

Beam Span (m)	6	9	12	15
Beam Section	UKB 356*127*33	UKB 406*178*60	UKB 457*191*98	UKB 610*229*125
Load Ratio	0.4	0.4	0.4	0.4
Connection Depth (mm)	260	290	320	410

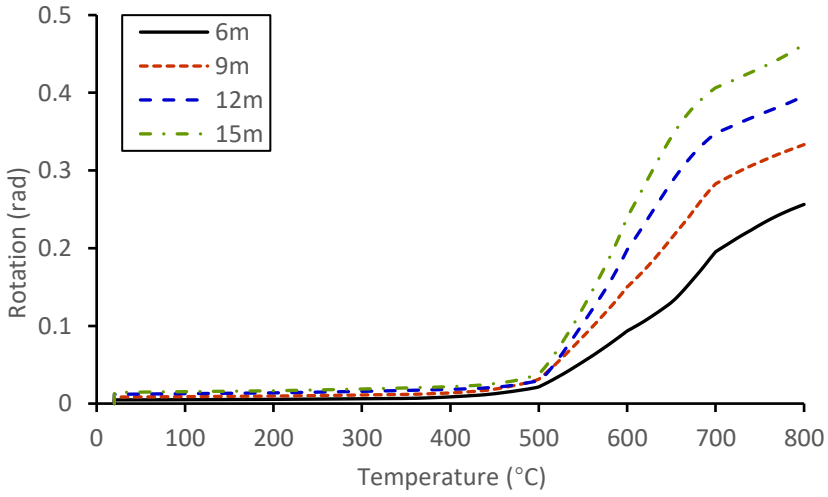

Figure 31. Rotation of connections for beams of different spans..

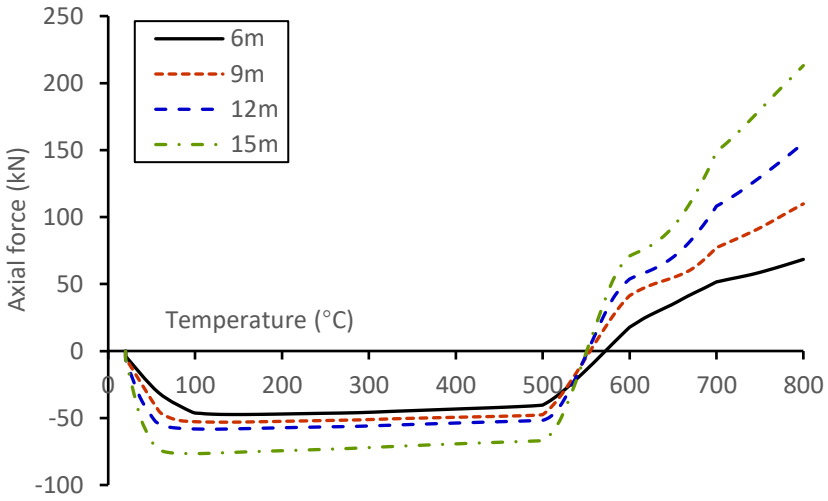

Figure 32. Axial force of beams of different spans.

7. CONCLUSION

This paper has proposed the design of a novel connection consisting of two connection pieces, each of which takes the form of a fin-plate, an end-plate and a cylindrical section which can provide additional ductility to reduce the probability of brittle failure. Tension/compression analytical models of the novel connection based on plastic theory and the virtual work principle have been developed. The rotational behaviour of the entire connection is simulated by pure tension or compression of individual connection strips, using the concept of the component-based method; the shear force between adjacent connection strips due to deformation compatibility might in future be considered as a safety factor.

Validations have been made against Abaqus simulations. A good consistency can be seen between tension/compression analytical models and Abaqus models at both ambient and elevated temperatures; this indicates that the proposed analytical model is able to predict the tension and compression behaviour of the connection.

Validations have been made against tensile and compressive experiments. A good correlation

has been found between the analytical models and experiments at ambient temperatures in both tension and compression quadrants.

A preliminary case study has been conducted to investigate the performance of the connection. Through the deformation process it can be seen that the cylindrical section provides additional ductility to accommodate large axial deformation caused by the horizontal movement of the connected beam. From the comparison of beam mid-span deflections under different boundary conditions, it can be concluded that the novel connection behaves like an idealized pinned joint. In general, the novel connection can provide the ductility required by the connected beam at both ambient and elevated temperatures, which means that compressive restraint forces generated by thermal expansion of the connected beam and catenary tension forces generated by the beam under very high temperature can be reduced. In this way, the fracture of connections, which may trigger progressive collapse of an entire structure in fire conditions, could be effectively prevented.

REFERENCES

[1] T. McAllister, G. Corley, World Trade Center Building performance study: Data collection, preliminary observations, and recommendations, Federal Emergency Management Agency, 2002.

[2] G.M. Newman, J.T. Robinson, C.G. Bailey, Fire safe design: A new approach to multi-storey steel-framed buildings, Steel Construction Institute, 2000.

[3] R.G. Gann, W.L. Grosshandler, H.S. Lew, R.W. Bukowski, F. Sadek, F.W. Gayle, J.L. Gross, T.P. McAllister, J.D. Averill, J.R. Lawson, Final Report on the Collapse of World Trade Center Building 7. Federal Building and Fire Safety Investigation of the World Trade Center Disaster (NIST NCSTAR 1A)*** DRAFT for Public Comments, in, 2008.

[4] J. Kruppa, Resistance au feu des assemblages par boulons haute resistance, CTICM, Puteaux, (1976).

[5] R. Lawson, Behaviour of steel beam-to-column connections in fire, Structural engineer, 68 (1990) 263-271.

[6] R. Lawson, Enhancement of fire resistance of beams by beam to column connections, Steel Construction Institute UK, 1990.

[7] L.C. Leston-Jones, The influence of semi-rigid connections on the performance of steel framed structures in fire, in, University of Sheffield, 1997.

[8] K.S. Al-Jabri, The behaviour of steel and composite beam-to-column connections in fire, in, University of Sheffield, 1999.

[9] T. Liu, Finite element modelling of behaviours of steel beams and connections in fire, Journal of Constructional Steel Research, 36 (1996) 181-199.

[10] S. Elsawaf, Y. Wang, P. Mandal, Numerical modelling of restrained structural subassemblies of steel beam and CFT columns connected using reverse channels in fire, Engineering Structures, 33 (2011) 1217-1231.

[11] L.S. da Silva, A. Santiago, P.V. Real, A component model for the behaviour of steel joints at elevated temperatures, Journal of Constructional Steel Research, 57 (2001) 1169-1195.

[12] S. Spyrou, Development of a component based model of steel beam-to-column joints at elevated temperatures, in, University of Sheffield, 2002.

[13] S. Spyrou, J. Davison, I. Burgess, R. Plank, Experimental and analytical investigation of the ‘compression zone’component within a steel joint at elevated temperatures, Journal of Constructional Steel Research, 60 (2004) 841-865.

[14] S. Spyrou, J. Davison, I. Burgess, R. Plank, Experimental and analytical investigation of the 'tension zone'components within a steel joint at elevated temperatures, Journal of constructional steel research, 60 (2004) 867-896.

[15] F.M. Block, Development of a component-based finite element for steel beam-to-column connections at elevated temperatures, in, University of Sheffield Sheffield, UK, 2006.

[16] F. Block, J. Davison, I. Burgess, R. Plank, Deformation-reversal in component-based connection elements for analysis of steel frames in fire, Journal of Constructional Steel Research, 86 (2013) 54-65.

[17] H. Yu, I. Burgess, J. Davison, R. Plank, Experimental Investigation of the Tying Capacity of Web Cleat Connections in Fire', in: The 5th European conference on steel structures, 2008.

[18] H. Yu, I. Burgess, J. Davison, R. Plank, Numerical simulation of bolted steel connections in fire using explicit dynamic analysis, Journal of Constructional Steel Research, 64 (2008) 515-525.

[19] H. Yu, I. Burgess, J. Davison, R. Plank, Development of a yield-line model for endplate connections in fire, Journal of Constructional Steel Research, 65 (2009) 1279-1289.

[20] H. Yu, I. Burgess, J. Davison, R. Plank, Experimental investigation of the behaviour of fin plate connections in fire, Journal of Constructional Steel Research, 65 (2009) 723-736.

[21] H. Yu, I. Burgess, J. Davison, R. Plank, Tying capacity of web cleat connections in fire, Part 1: Test and finite element simulation, Engineering Structures, 31 (2009) 651-663.

[22] H. Yu, I. Burgess, J. Davison, R. Plank, Tying capacity of web cleat connections in fire, Part 2: Development of component-based model, Engineering structures, 31 (2009) 697-708.

[23] H. Yu, I. Burgess, J. Davison, R. Plank, Experimental and numerical investigations of the behavior of flush end plate connections at elevated temperatures, Journal of Structural Engineering, 137 (2010) 80-87.

[24] S.-S. Huang, B. Davison, I.W. Burgess, Experiments on reverse-channel connections at elevated temperatures, Engineering structures, 49 (2013) 973-982.

[25] G. Dong, I. Burgess, J. Davison, Application of a general component-based connection element in structural fire analysis', in: Proc. 11th Int. Conference on Steel, Space and Composite Structures, Qingdao, China, 2012.

[26] G. Dong, I. Burgess, B. Davison, R. Sun, Development of a general component-based connection element for structural fire engineering analysis, Journal of Structural Fire Engineering, 6 (2015) 247-254.

[27] I. Burgess, J.B. Davison, G. Dong, S.-S. Huang, The role of connections in the response of

steel frames to fire, Structural Engineering International, 22 (2012) 449-461.

[28] E. BSI, 3: design of steel structures: part 1-8 design of joints, BS EN 1993-1-8, London: British Standard Institution, 18 (2005).

[29] M.R. Horne, Plastic Theory of Structures: In SI/metric Units, Elsevier, 2014.

[30] P. Bhatt, Structures, Addison-Wesley Longman Limited, 1999.

[31] CEN, Eurocode 3: Design of steel structures—Part 1-8: Design of joints, (2005).

[32] W. Gittleman, Bending Moments in a Circular Ring by the Column Analogy, Aircraft Engineering and Aerospace Technology, 18 (1946) 122-125.

[33] J. Prescott, Applied elasticity, Longmans, Green and Co., 1924.

[34] J.L. Krahula, " Out-of-Plane Bending of a Uniform Circular Ring, in: International Association for Bridge and Structural Engineering, 1965.

[35] S. Kalawadwala, Investigation of the performance of innovative connection under hazard loading, (2018).